Serb. Astron. J. № 177 (2008), 87 - 99 **UDC 523.94–78**
DOI: 10.2298/SAJ0877087A Original scientific paper

PROPAGATION OF HIGH FREQUENCY WAVES IN THE QUIET SOLAR ATMOSPHERE

A. Andić[1,2]

[1] *HiROS, School of Physics and Astronomy, College of Engineering and Physical Sciences, The University of Birmingham, Edgbaston, Birmingham, B15 2TT, UK*

[2] *Astrophysics Research Centre, School of Mathematics and Physics, Queen's University, Belfast, BT7 1NN, UK*

E–mail: *andic@bison.ph.bham.ac.uk*

(Received: August 22, 2008; Accepted: October 1, 2008)

SUMMARY: High-frequency waves (5 mHz to 20 mHz) have previously been suggested as a source of energy accounting for partial heating of the quiet solar atmosphere. The dynamics of previously detected high-frequency waves is analysed here. Image sequences were taken by using the German Vacuum Tower Telescope (VTT), Observatorio del Teide, Izana, Tenerife, with a Fabry-Perot spectrometer. The data were speckle reduced and analysed with wavelets. Wavelet phase-difference analysis was performed to determine whether the waves propagate. We observed the propagation of waves in the frequency range 10 mHz to 13 mHz. We also observed propagation of low-frequency waves in the ranges where they are thought to be evanescent in the regions where magnetic structures are present.

Key words. SUN: oscillations – SUN: atmosphere

1. INTRODUCTION

An ongoing debate about the heating mechanism of the solar atmosphere and the role of waves in it (Ghosh 2002) provide the motivation for studying the dynamics of high-frequency waves. This work is a continuation of the wave analysis, parts of which are already presented in the previous papers (Andic 2007a,b and Andjic 2006), and focuses on waves with frequencies from 1 mHz to 22 mHz. Special attention will be given to interpretation of the results for the frequencies above 10 mHz.

The temperature of the solar atmosphere varies from a minimum value in the photosphere (around $4 \cdot 10^3$K) to a maximum typically found in the corona ($1 \cdot 10^6$K). What supplies the energy necessary to give rise to this temperature difference is still under discussion. Some authors claim that high-frequency waves carry the necessary energy (Ulmschneider 1971a,b, 2003, Stein and Leibacher 1974, Kalkofen 1990, 2001, Wedemeyer-Böhm et al. 2007), while others claim that low-frequency ones are the main source (Wang et al. 1995, Jefferies et al. 2006).

Recent work by Fossum and Carlsson (2005) and Andic (2007a) found no observational evidence for flux energetic enough to promote the acoustic heating proposed for high-frequency waves (Ulmschneider 1971a,b, 2003, Stein and Leibacher 1974, Kalkofen 1990, 2001). Following these observational results, Wedemeyer-Böhm et al. (2007) present calculations using 3D models (Wedemeyer et al. 2004)

and state that high-frequency acoustic waves do in fact have a role in the energy supply to the corona.

A simple assumption is that acoustic waves will propagate upward, form a shock and therefore dissipate energy. This explanation assumes that the magnetic field is not required for the propagation of acoustic waves. Works by Rosental et al. (2002) and De Pontieu et al. (2004) have shown otherwise. Rosental et al. (2002) presented 2D model of wave propagation in the presence of a magnetic field, and they concluded that the presence of magnetic fields significantly complicates the waves and their associated dynamic. Jefferies et al. (2006) state that waves which were previously considered to be evanescent (Thio 2006) can propagate when magnetic fields are present.

2. OBSERVATIONS

The data presented here are the same as already used in the previous papers (Andic 2007a,b, Andjic 2006).

The spectral lines Fe I 543.45 nm ($g_L = 0$) and 543.29 nm ($g_L = 0.335$) were taken and 2D spectroscopy was performed using the German Vacuum Tower telescope (VTT), Observatorio del Teide, Izana, Tenerife, with the Fabry-Perot spectrometer. The data were obtained during the mornings of 22 and 24 June 2004, with excellent seeing conditions and with the use of an adaptive optics system (Berkefeld et al. 2003). The solar disk centre was targeted and the data were obtained in bursts of images. The exposure time of an individual image was 30ms and the cadence between successive images was 0.25s. The time to scan the line profile was 28.4s. This gave us a Nyquist frequency of 17.6 mHz (Grenander 1959, various chapters). The field of view was 38" × 20" and the data sequence obtained on 22.06.2004 (DS1) lasted one hour, while the data sequence obtained on 24. 06. 2004 (DS2) lasted 40 minutes. The duration of the sequences was chosen to improve reliability of the analysis of results (Chatfield 2003, various chapters).

No data were acquired specifically in support of the VTT observations, so we are unable to specify the exact state of the photospheric magnetic field during the observations. Nevertheless, the MDI instrument on SOHO was running in a mode where full disk magnetograms were obtained every 96 minutes. Comparison of the MDI with the VTT data indicates that the central VTT pointing was similar to MDI, with an error of ±10". A G-band was used to ensure that the correct solar features were observed, i.e. no bright points in DS1 and an abundance of magnetic structures in DS2.

The data set DS1 has been taken in areas where no visible magnetic structuring was present. The MDI data revealed that the region scanned within the VTT field of view was in a typical quiet region, mostly unipolar (DS1, from 22. 06. 2004), with a moderately intense magnetic network in the data set DS2, from 24.06.2004. A filtergram of the data set DS2 shows an abundance of G-band bright structures.

Figs. 1 and 2 reveal the magnetograms taken by the MDI instrument at times corresponding to the time of the observations. It is obvious that both data sets are taken near the solar disc centre with no significant difference in the inclination angle of the lines of sight.

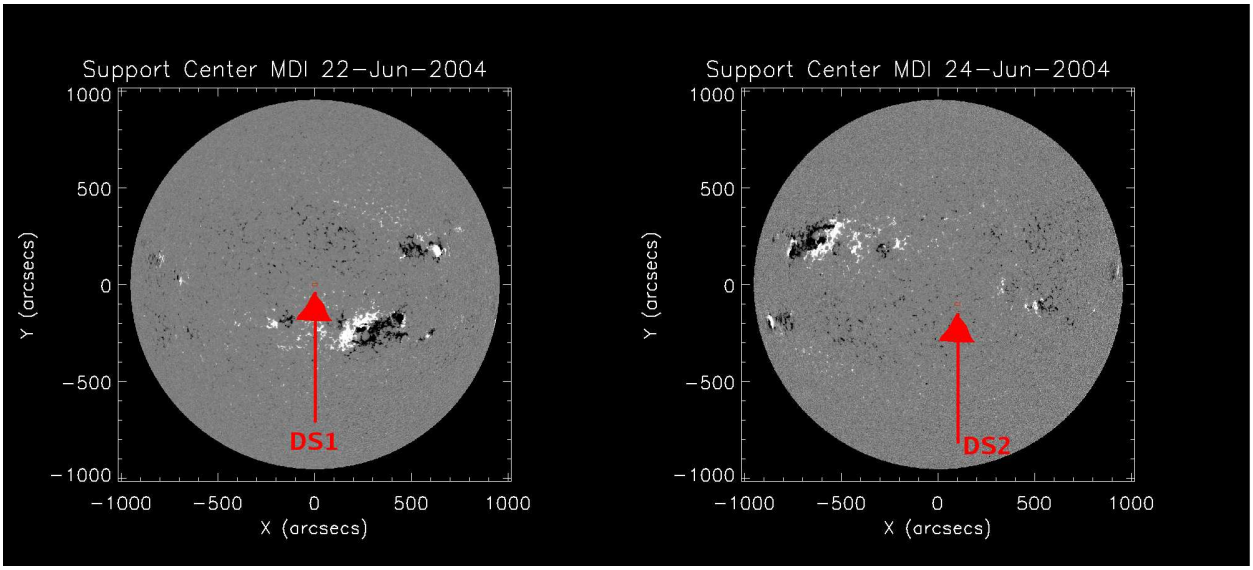

Fig. 1. *The magnetogram of the whole solar disc from the SOHO instrument, MDI. The left panel represents the magnetogram taken on 22.06.2004 just before the observations commenced, while the right panel shows the magnetogram taken on 24.06.2004. The tips of the arrows on both panels point at the location of the used field of view.*

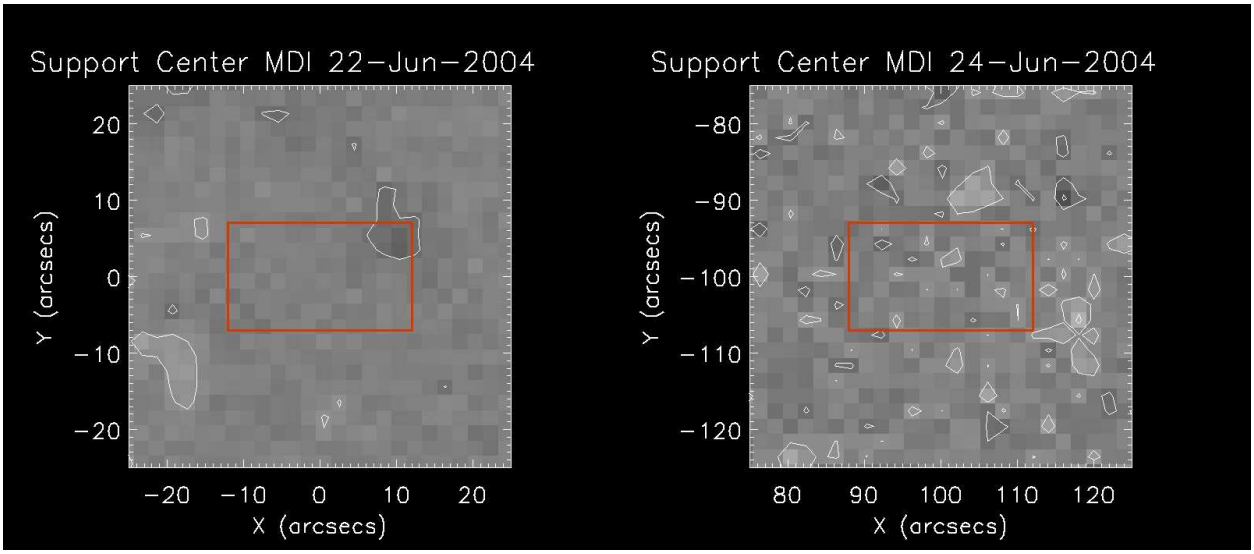

Fig. 2. *The zoomed part of Fig. 1. The left panel represent data set DS1 and the right panel DS2. The superimposed white contours are curves marking a magnetic field of 10 Gauss. The red squares represent the approximate locations of the field of view.*

Based on these data, we conclude that the VTT time series data set DS1 corresponds to typical quiet Sun conditions, while DS2 has part of the magnetic network in the field of view (Phillips 1992).

3. DATA REDUCTION AND THE METHODS OF ANALYSIS

The data were reduced using the methods already explained in the previous papers (Andic 2007a,b and Andjic 2006). As a consequence of the reduction procedure and of the implemented subsequent coalignment of the reconstructed images, the field of view and duration of the data sets were reduced. Consequently, data set DS1 has a field of view 32.3" ×14.4" with a duration of 52.54 min, while data set DS2 has a field of view 29.3" × 7.4" with a duration of 33.13 min after reduction. We estimate the formation layer of the line cores (Phillips 1992, del Toro Iniesta 2003). We based the estimate for the formation height of the Fe I 543.45 nm and 543.29 nm line cores on the location of optical depth unity at the central wavelength as calculated from a 3-D radiative-hydrodynamic simulation of Asplund et al. (2000). This method is described in detail in the paper by Shchukina and Trujillo Bueno (2001). The formation heights in NLTE are 258.5 km and 588.7 km for Fe I 543.29 nm and Fe I 543.45nm, respectively (N. Shchukina, private correspondence). The wavelet analysis used here is also described in detail in the previous papers (Andic 2007a,b and Andjic 2006). The following criteria are applied to remove spurious oscillations:

* The signal curve is tested against spurious detections of power that may be caused by Poisson noise, assuming that it is normally distributed and follows a χ^2 distribution with two degrees of freedom. A confidence level of 99% is calculated by multiplying the power in the background spectrum by the values of χ^2 corresponding to the 99th percentile of the distribution (Torrence and Compo 1997, Mathioudakis et al. 2003).
* The signal curve is compared with a large number (1500) of randomised time series with an identical counts distribution. By comparing the value of power found in the input signal curve with the number of times the power transform of the randomised series produced a peak of similar power, the probability of detecting non-periodic power is calculated for the peak power at each time-step. This information is used to remove all spurious power from our results. (Banerjee et al. 2001)
* All oscillations of duration less than 1.5 cycles were excluded by comparison of the width of the peak in the wavelet power spectrum with the decorrelation time. This is done to distinguish between a spike in the data and a harmonic periodic component at the equivalent Fourier frequency, thus defining the oscillation lifetime at the period of each power maximum as the interval of time from when the power supersedes 95% significance until it subsequently dips below 95% significance (McAteer et al. 2004). To obtain the number of cycles, the lifetime is divided by the period.
* All oscillations with a power of less than 15% of the maximum power in the time sequence were excluded. Wavelet analysis with the Morlet wavelet as the mother wavelet has a tendency to also detect spurious oscillations. Wavelet analysis is performed for the flat-fields, which contain noise, and the power of

the oscillations detected is noted and compared with those found in the dataset. This gives us a lower limit to the power of the observed oscillations.

* All oscillations with periods above 788.1 s (DS1) and 496.95 s (DS2) were excluded, since they might be due to edge effects arising from the finite time span of our data.

To study the propagation characteristics of the detected waves (Andjic 2006, Andic 2007a,b), wavelet phase coherence analysis is used (Bloomfield et al. 2004). When the power contained in the time series is studied, differences between traditional Fourier analysis and wavelet analysis are small. Fourier analysis, without timing information, has marginally different confidence levels when compared to wavelet analysis averaged over time.

However, the phase relations between the wave packets can differ in time or with a change in the local topology. These changes will be lost in the Fourier analysis due to the lack of timing information. This is mostly because phase can take negative values, while the power is always positive. Therefore, wavelet analysis is applied in this study. In the work by Bloomfield et al. (2004) a detailed description of this method is given. The equations used for the calculation of the phase difference and the phase coherence are given in Table 1. in the work by Bloomfield et al. (2004). For pure noise this procedure yields positive coherence. Only results with a coherence above 0.6 can be regarded as significant.

Phase difference and phase coherence (Davis 2000, various chapters) are calculated using the intensity and velocity signals from both line cores. Velocity signals were obtained from the spectral line bisector shift (Andic 2007a,b and Andjic 2006). This makes possible to form the phase differences between velocity-velocity (V-V) signals, velocity - intensity (V-I) signals and intensity - intensity (I-I) signals. Signals are chosen from the same spatial location (i.e. the same pixel in the field of view). For V-V and I-I phase difference calculations, signals are taken from the different spectral lines, while V-I phase differences are calculated from the same spectral line. This means that signals used for the V-V and I-I phase difference calculations are separated from each other by the height difference of the line cores, in addition to the constant 13.5 s gap caused by the scan time of the observed line profiles.

In order to compare the results with previous work, phase difference spectra are formed using the time-averaged phase differences (Fig. 3). The phase difference spectra are formed so that an upward propagating wave leads to a positive phase difference. The phase differences are presented in a weighted diagram, where the weighting is applied per sample by utilising a cross-power amplitude $\sqrt{P_1 P_2}$. Furthermore, they are binned into greyscale plots that are normalised to the same maximum per frequency bin (Lites and Chipman 1979). Fig. 4 shows the observed V-V phase lag between the velocity fluctuations of the Fe I 543.29 nm and Fe I at 543.45 nm lines. The coherence presented with each phase spectrum is obtained by averaging the mean time-averaged coherence (Fig. 3, panel Time av. Coherence) over all the processed signal curves.

4. RESULTS

In the context of periodic phenomena, phase angle is synonymous with the phase. We calculate the phase using as the reference point the oscillatory signal observed in one of the spectral lines; therefore, the phase difference is synonymous with the phase angle in this work. The term phase spectrum represents distribution of the phase angle (i.e. phase difference) arranged in a progressive series according to the frequency. The calculated phase spectra, in both data sets, show that the observed high-frequency waves do propagate. Fig. 3 represents the result of the phase analysis using the wavelets on a pair of curves from the data set DS2. The panels marked with LC1 Power and LC2 Power (where LC stands for the light curve), present the results of the wavelet power transforms. Lighter shaded regions correspond to an increased wave power. The contours indicate 95% confidence levels, while crosshatched areas mark the cone of influence (COI) where edge effects can be important (Torrence and Compo 1997, Bloomfield et al. 2006). The panel marked with Cross-wavelet Power represents the cross-wavelet power transform of both curves (in this case velocity curves), LC1 and LC2. The panel labelled with Phase Difference presents full time series wavelet phase difference transforms as a function of time (abscissa) and wave frequency (ordinate). The superimposed contours indicate 10% coherence exceedance levels, while the crosshatched area is COI. The panel marked as Time av. Phase Difference shows time-averaged phase differences (ordinate) from the panel Phase Difference, as a function of the wave frequency (abscissa). Midpoints correspond to the mean temporal phase difference. The panel marked with Coherence is the full time series wavelet phase coherence transform. Markings are the same as for the 'Phase Difference' panel. The 'Time av. Coherence' represents time-averaged phase coherence (ordinate) of coherence as a function of wave frequency (abscissa), where the dashed line marks mean coherence. The 'Phase Difference' panel shows the propagation of the high-frequency waves in different directions. Lighter shades mark upward propagation. A detailed explanation of how this plot is constructed is presented in the work by Bloomfield et al. (2004).

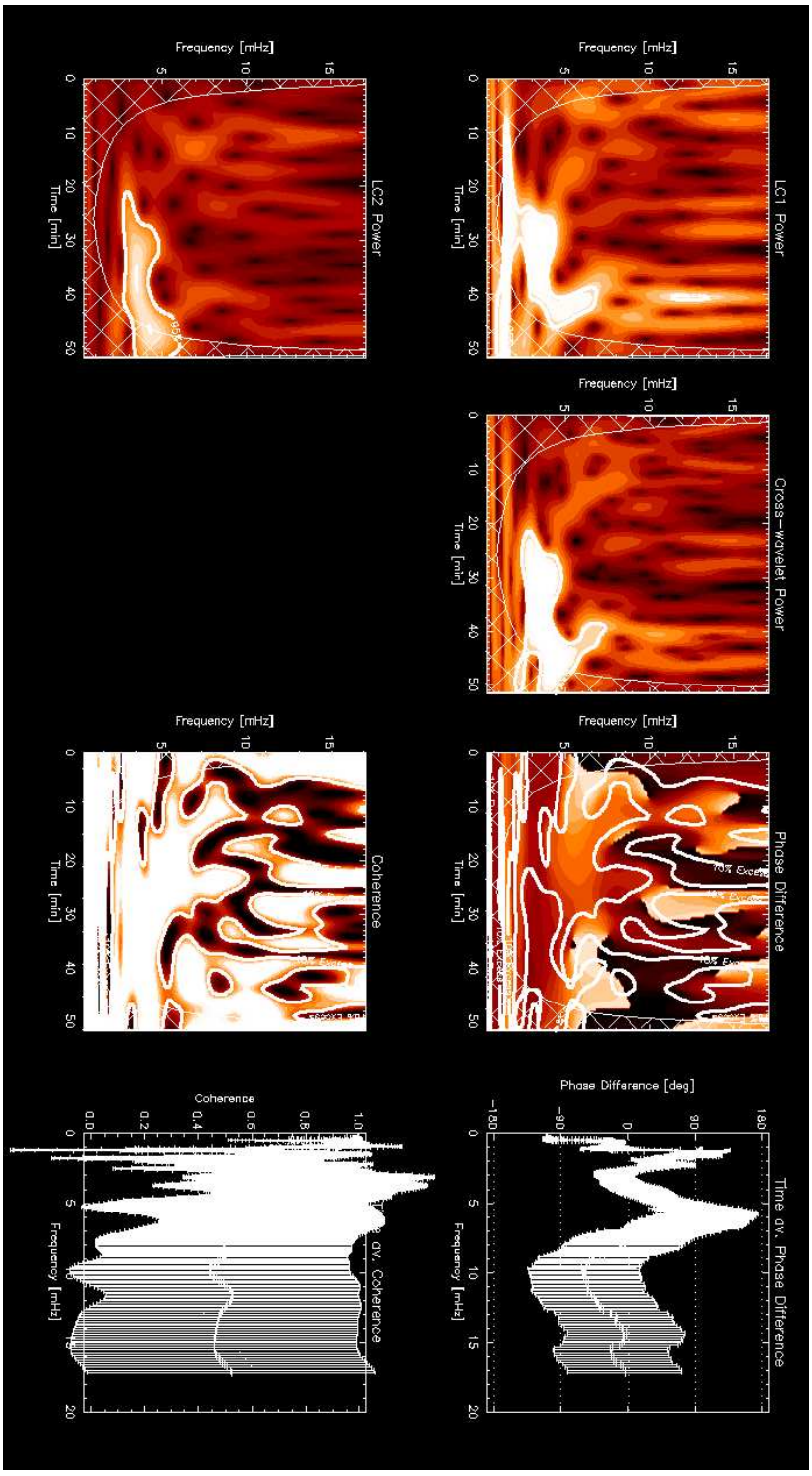

Fig. 3. *Result of wavelet phase coherence analysis for the data set DS2. The wavelet analysis of both signal curves are shown in the panels marked with LC1 and LC2 Power. The panel marked Cross-wavelet Power shows the cross power for the both curves. The phase difference and the corresponding coherence are given in the panels marked with the Phase difference and Coherence. Also shown in the last two panels are the phase difference and coherence averaged over time.*

Figs. 4 and 5 show that the observed direction of the propagation is upwards. Several phase spectra were calculated to obtain as much information as possible about the dynamics of the studied areas. The following results are presented separately for both data sets.

4.1. Data set DS1

For this dataset 46512 signal curves were compared. The top panel of Fig. 4 presents the phase spectrum calculated between velocity fluctuations (V-V) at the cores of two observed lines. The phase difference spectrum shows that the five-minute waves do not propagate, and displays an upward propagation at higher frequencies up to $f \approx 13$ mHz. The coherence is very small below 1 mHz, where the disregarded frequencies are located, above that it varies between 0.7 and 1. The phase differences for the frequencies below 1.26 mHz can be caused by the edge effects due to the finite time span.

The top panel in Fig. 5 presents the phase spectrum calculated between intensity fluctuations (I-I) at the cores of two observed lines. For this phase spectrum, the coherence distribution varies much more than for the V-V spectrum. It shows a decrease in the frequency range $4 - 8$ mHz to a value close to 0.6. After that, we see the positive phase difference increasing. This indicates that the high-frequency waves observed in the intensity maps do travel upwards. This trend is visible even for the waves close to the Nyquist frequency, although in the frequency range above 13 mHz there is a sudden drop in phase difference, even a tendency for negative phase differences as well. The coherence distribution in this range has several peaks and drops. It is significant to note that inthe areas where the coherence drops the positive phase difference is not dominating the spectra.

The solid black line in Fig. 6 shows average velocity distribution calculated with the V-V phase spectra. The positive (negative) velocities mark upward (downward) propagation. On the average, there is no propagation for the waves in the frequency range around 5 mHz. All other frequencies show propagation. The upward propagation dominates this curve, despite a strong negative maximum near a frequency of 15 mHz. After averaging over the whole frequency range we get a propagation velocity of 26.26 m/s, which demonstrates the prevalence of the upward propagation. The solid black line in Fig. 7 shows the average velocity distribution calculated with the I-I phase spectra. At lower frequencies we can observe that the waves with frequencies around the cut-off frequency do propagate. The upward propagation dominates this curve. Averaged over the whole frequency range the velocity is 19.01m/s.

Fig. 8 shows the phase spectrum calculated between the velocity and intensity signals (V-I). The top left panel represents results for the spectral line Fe I 543.45 nm. On the average, the phase spectra show that oscillations appear first in velocity curves and then in intensity curves. This trend is apparent

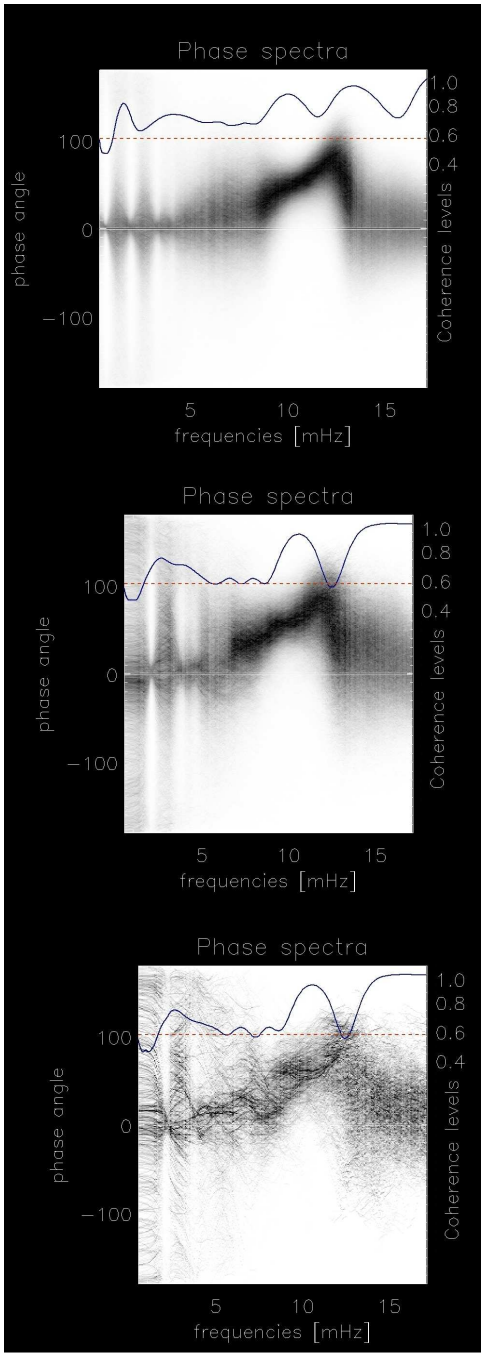

Fig. 4. *The V-V phase difference and the corresponding coherence distribution for the calculated phase. The top panel represents the phase difference calculated for the data set DS1. The other two panels represent the phase difference from the DS2 data set. The bottom panel represents the phase difference for the locations where the bright points appear for at least half of the duration of a time sequence. The middle panel represents the rest of the field of view. On each panel the corresponding average coherence distribution is plotted. The dashed red lines represent coherence levels of 0.6.*

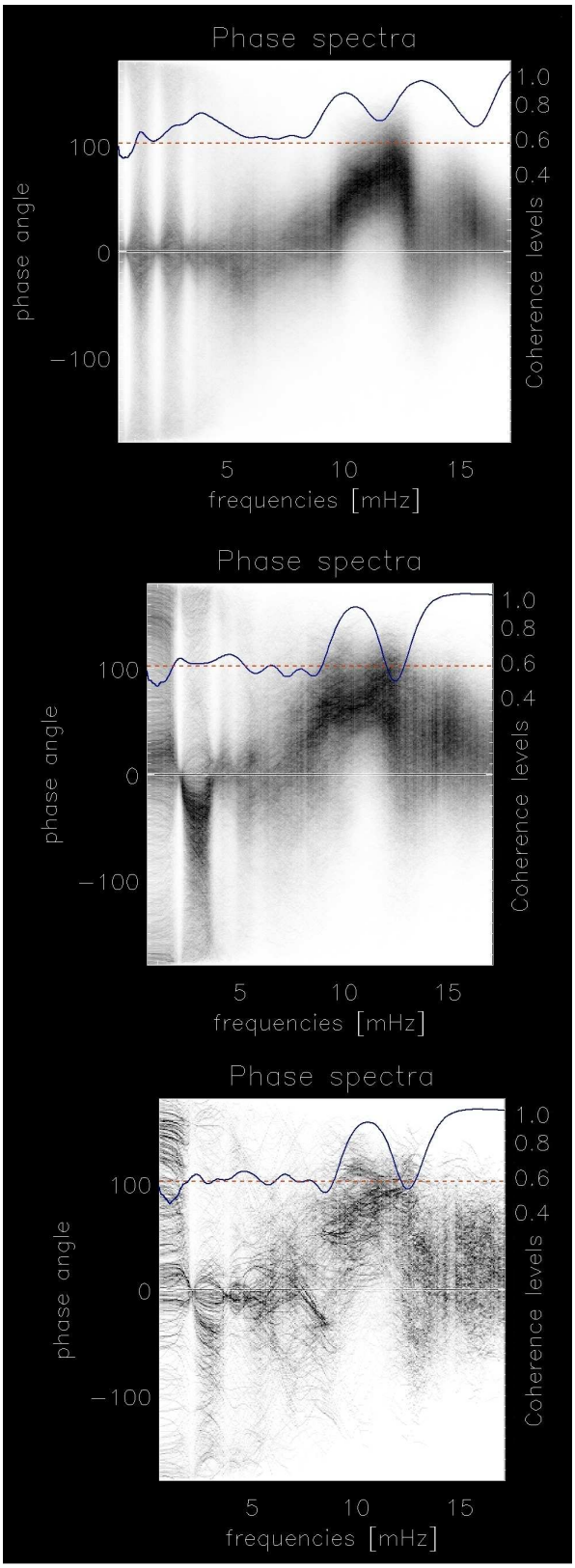

Fig. 5. *Same as Fig. 4 but for the I-I phase difference.*

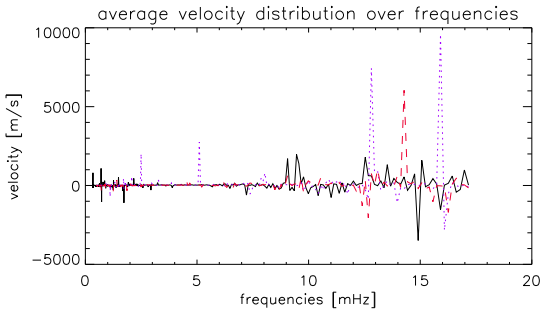

Fig. 6. *The average velocity distribution over the analysed frequency range calculated with V-V phase difference. The solid black line represents distribution for the data set DS1; the dashed red line and the dotted purple line represent the data set DS2. The dotted purple line represents results from the parts of the field of view where magnetic structures in DS2 appear for at least half of the duration of the time series, while dashed red line represents the results for the rest of the field of view.*

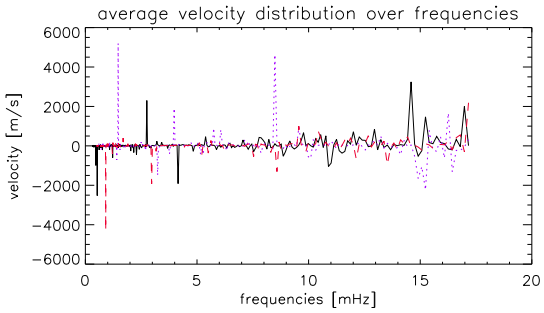

Fig. 7. *Same as in Fig. 6 but calculated with the I-I phase difference.*

from the concentration in the frequency range of 8 mHz – 15 mHz. The rest of the phase spectra are ambiguous.

The top right panel of Fig. 8 presents the phase spectrum which is calculated between the velocity and intensity signal (V-I) for the spectral line Fe I 543.29 nm. The phase difference is positive at most frequencies, indicating that signals appear first in the velocity and then in the intensity curves. The coherence distribution is lowest for this phase spectra. The coherence distribution tends to drop in value when the intensity curves are analysed. This might be caused by the fact that intensity curves tend to have more spurious oscillations than velocity curves (Carlsson, private communication).

4.2. Data set DS2

For this dataset 21682 signal curves were compared. The phase differences for the frequencies below 2 mHz can be caused by the edge effects due to the finite time span. These frequencies are not taken into consideration in this analysis. Results for this

data set tend to follow the general trend from the previous data set above the frequency $f \approx 7$ mHz. The middle and bottom panels in Fig. 4 illustrate this trend. However, at lower frequencies the phase difference is approximately zero. Moreover, the coherence distribution is relatively low and varies much more than for the previous data set. The phase difference is calculated separately for the areas where the bright points appear (bottom panel) and separately for other locations (middle panel). Except the obvious lower number of curves there is no difference in the behaviour.

The real difference can be noticed for the average velocity distribution. The dotted purple line in Fig. 6 shows the average velocity distribution calculated with V-V phase spectra for the areas where the bright points appear. In the frequency range below 6 mHz the average velocities show that there is more propagation for areas where the bright-points appear. Also, in the high-frequency range, above 12 mHz, there is a tendency for greater velocities. The dashed red line represents the average velocity distribution for the rest of the field. This line shows that the behaviour in the rest of the field is more similar to the behaviour of DS1 (solid black line). Averaged over the whole frequency range the velocity is: 74.43 m/s for areas where the bright points appear and 23.88 m/s for the rest of the field of view.

An average velocity distribution calculated with I-I also shows different behaviour in the lower-frequency range for different fields of view. The field with the intense magnetic flux concentrations (dotted purple line, Fig. 7) shows different tendencies for propagation with greater velocities. The rest of the field of view (dashed red line) shows behaviour similar to DS1 (solid black line). Averaged over the whole frequency range the velocity is 22.52 m/s for areas where the bright points appear and 10.47 m/s for the rest of the field of view.

The phase spectrum for the intensity waves shows similar behaviour to that for DS1. Where the coherence is reasonably high we observe that the waves do travel upward (middle panel in Fig. 5). The overall coherence is much lower than for the previous data set. The bottom panel represents results for the areas where the bright points appear. Apart from the obvious smaller number of curves there is no difference in trend.

The phase spectrum V-I calculated for the spectral line Fe I 543.45nm is presented in the middle and bottom rows of Fig. 8. Here the coherence is highly variable and lower than for the DS1. The middle panels show trends that are similar to the top panels (DS1). For the spectral line Fe I 543.45nm (left middle panel of Fig. 8), it is obvious that waves appear first in the velocity and then in intensity curves for the frequency range $8 - 13$ mHz. The rest of the spectra are more ambiguous. The spectral line Fe I 543.29 nm (middle left panel of Fig. 8) shows a slightly larger concentration of the phase difference in a positive range for the frequencies above 5 mHz, similar to those observed for DS1 (top left panel of Fig. 8). Both show the tendency for waves to appear first in the velocity and then in the intensity curves.

V-I phase spectra, in the right bottom panels of Fig. 8, are ambiguous due to the small number of curves. The tendency for the positive phase difference is clearly noticeable only above 11 mHz. The left bottom panel of Fig. 8 shows behaviour similar to the left middle panel.

5. DISCUSSION AND CONCLUSIONS

The data sets used in this work were also used in the previous papers (Andic 2007a,b and Andjic 2006). The possible problems in observing the high-frequency waves were discussed in detail in these papers. To observe the wave propagation one has to observe the wave at two different places in space-time. In this work we observed the waves that leave signatures of propagation in the cores of two spectral lines. The signals we observed do appear first in the line core of Fe I 543.29 nm and then in the line core of Fe I 543.45 nm. This should indicate wave propagation. To interpret these observations we used the model described in Asplund et al. (2000), and on the basis of this model we used the method described in Shchukina and Trujillo Bueno (2001) to obtain the atmospheric heights at which the observed spectral lines are formed. However, as described in several chapters of the book by del Toro Iniesta (2003), the assumption that a certain spectral line is formed at a certain atmospheric height is valid only in the used atmospheric model. Therefore, we have to state that the interpretation and all quoted velocity values are heavily dependent on the model and they are correct only as much as the assumptions of the model. An additional problem is the assumption that the signals observed in both line cores are separated. Only under that assumption can the observed phase difference actually indicate the wave propagation. Unfortunately, this assumption is also based on the atmospheric model and the assumed independence of the formation of the different spectral lines. Therefore, this assumption introduces similar uncertainty as formation heights. In both data sets no propagation for the low-frequency waves - below 5 mHz - was observed. This is expected since most of the models (Ulmschneider 1971a,b, 2003, Stein and Leibacher 1974, Kalkofen 1990, 2001, Wedemeyer-Böhm et al. 2007) predict that in the lower Solar atmosphere waves with such frequencies will be evanescent, i.e. non-propagating. This work concentrates only on the waves propagating in the direction parallel to the line of sight. This preference is initially chosen due to previous works on the modeling of the photospheric magnetic field. Subsurface magnetic fields are continually stretched and distorted by convective flows (Emonet and Cattaneo 2001) resulting in the emergence of flux bundles in the photosphere. Newly emerged fields are swept towards the boundaries of granules and super-granules where they interact with pre-existing magnetic fields. In mixed-polarity regions, with mean flux density of a few Gauss, the recycling time scale is about 40 hours (Title and Schrijver 1998). The flux tubes are less dense than their surroundings and therefore buoyant. This buoyancy

keeps the flux tubes nearly vertically oriented in the photosphere. A flux tube with a weak magnetic field in thermal and hydrostatic equilibrium with its surroundings is unstable against vertical displacements of plasma within the tube (Parker 1978). This implies that in the quiet photosphere most of the magnetic flux tubes are vertical (i.e. parallel to the line of sight). However, recent studies have shown complexity of the magnetic fields of the photosphere and chromosphere. Flux tubes, which usually channel the oscillations upward, have different propagation conditions, angle of the spread and orientation at the heights analysed here. (van Ballegooijen and Hasan 2003, Fig. 6). Due to this complexity of the magnetic fields in the photosphere and chromosphere, it is not clear what percentage of the oscillations propagating upward, which can be determined with observations along the line of sight, is normal to the solar surface.

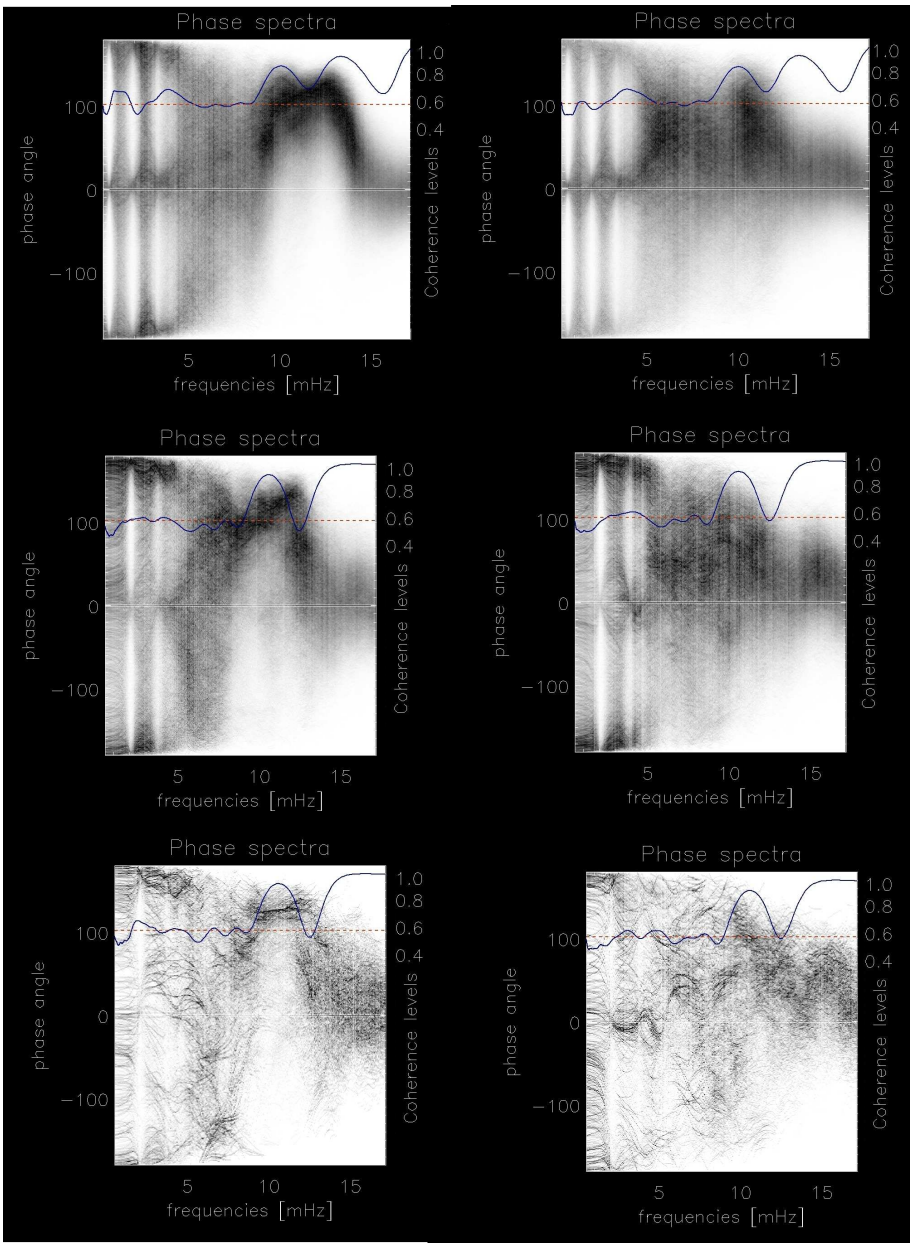

Fig. 8. *The V-I phase difference and the corresponding coherence distribution for the calculated phase, as in Fig. 4. Left column represents phase difference calculated for the spectral line Fe I* 543.45 *nm and the right one for the spectral line Fe I* 543.29 *nm. The top row represents results from the data set DS1, while the bottom row represents the results from the reduced field of view, where magnetic structures in DS2 appear for at least half of the duration of the time series and the middle row from the rest of the field of view for DS2.*

To fully analyse waves propagating along the inclined flux tubes, the information about the magnetic field is necessary. However, MDI does not give us information on the resolution comparable with our ground-based data. Therefore, we analysed only the waves propagating parallel to the line of sight. To analyse the rest of the waves, one needs high-resolution magnetograms.

5.1. Data set DS1

In this data set the wave propagation was observed in the frequency range from $\approx$ 7 mHz to 13 mHz. Although Krijger et al. (2001) claim that near this range there is steepening into weak shocks of acoustic waves on the way up, the resolution of the spectral lines in that area of the field of view makes it impossible to confirm this conclusion in our case. Since our Nyquist frequency is 17 mHz, close to this frequency we have only two points per wave and this introduces uncertainty into the calculated phase differences for those frequencies. Also, the steepening which Krijger et al. (2001) observed starts in the range where we still observe a clear upward propagation in V-V maps (top panel of Fig. 4). There is the possibility that the drop in the phase difference after 12 mHz and subsequent reduction in the concentration of the phase differences is due to an increase in the propagation velocities of the waves. This matter will be resolved with more sensitive instruments. The propagation is less clear in the I-I spectra (top panel of Fig. 5), where there is additional phase difference concentration around 15 mHz.

Moreover, top panel of Fig. 5 shows that around a frequency of 4 mHz there is a very slight tendency towards negative phase differences just after 5 mHz, which indicates that the observed waves are travelling downwards. This is confirmed by the average propagation velocity distribution that shows a negative peak in the black curve in Fig. 7. Both findings indicate that in this range there is a tendency for downward waves. However, the V-V phase difference in the top panel of Fig. 4 does not show such a trend. This might indicate that either the sources of the velocity and intensity signals around this frequency range are not the same or there is an influence of NLTE effects in the core of the higher spectral line, Fe I 543.45 nm.

The top two panels of Fig. 8 show the phase spectrum calculated between the velocity and intensity signal (V-I) for the spectral lines Fe I 543.45 nm (top left panel) and Fe I 543.29 nm (top right panel). These panels show that the phase spectrum for the spectral lines tend to concentrate in a positive range (angle values from 40 to 100). This trend is obvious for the frequency ranges 8 mHz – 14 mHz in the top left panel of Fig. 8. The top right panel does show similar tendencies for the spectral line Fe I 543.29 nm. Both panels indicate that the observed waves appear first in the velocity and then in the intensity curves.

5.2. Data set DS2

Results for this data set tend to follow the general trends seen in the other data set in the frequency range 6 mHz – 13 mHz (middle panel of Fig. 4). The same trend is visible for intensity waves where the frequency range 7 mHz – 12 mHz shows a clear propagation (middle panel of Fig. 5).

Here 21682 signal curves were compared. We investigate whether the intense magnetic flux concentrations can cause the differences noted in the phase spectra. Separate phase differences were calculated for the areas where the magnetic flux concentrations appear more often than in the rest of the field of view (at least for a half of duration of the time series). Phase difference trends for those areas are similar to the rest of the field of view, as shown in the bottom panels of Figs. 4 and 5. The only apparent difference arises from the smaller number of the analysed curves. The difference between areas with a different magnetic flux concentration is more noticeable in Figs. 6 and 7. Both diagrams show that the average propagation velocity distribution tends towards greater values for the areas where the magnetic flux concentrations appear more often (dotted purple line).

The middle and bottom rows of Fig. 8 show the phase spectra for the V-I signal. Both show the tendency for waves to appear first in the velocity and then in the intensity curves. The middle panels show trends that are similar to the top panels (DS1). The bottom rows show clear differences because of the smaller number of analysed curves. This difference is especially noticeable for the right bottom panel, where the phase spectra tend towards a positive phase difference is clearly noticeable only above the frequency of 11 mHz.

Magnetic flux tubes, which usually channel the waves upward, have different propagation conditions, angles of the spread and orientation at the heights analysed here (van Ballegooijen and Hasan 2003, Fig. 6). This might explain the higher phase velocities registered for the waves from the area where magnetic structures are appearing for at least half of the time series duration. Work by De Pontieu et al. (2004) confirms that inclined flux tubes are the cause of the leak of p-mode energies to higher layers of the solar atmosphere. This might result in the noted positive phase velocity in the frequency ranges where one expects evanescent waves. Also, the work by Berger et al. (2004) states that the magnetic field in the plage region is concentrated in complex structures, which are generally not composed of discrete magnetic flux tubes. This might explain why we do not observe typical behaviour for evanescent waves (Deubner and Fleck 1989, 1990, Fleck and Deubner 1989, Deubner et al. 1990) in our phase spectra for lower-frequency waves.

5.3. Both data sets

Krijger et al. (2001) claim that registered high-frequency waves do propagate and that phase spectra tend to lose coherence and spread for higher frequencies because of the steepening into weak shock of acoustic waves on the way up. The behaviour of the phase differences analysed here follows this pattern (Figs. 4 and 5). However, the frequency ranges of the observed waves which propagate and which lose coherence differ slighty from those found

by Krijger et al. (2001). We observe propagation in the range 6 mHz – 13 mHz for velocity signals and 8 mHz – 13 mHz for intensity signals. The phase differences noted here are also larger than in Krijger et al. (2001). The larger phase differences might indicate detection of faster waves. On the other hand, the heights that are sampled in this work (258.5 km and 588.7 km for Fe I 543.29 nm and Fe I 543.45 nm, respectively) are different from the ones sampled by Krijger et al. (2001). In the work by Krijger et al. (2001) the difference between sampled heights is approximated as being 140 km while here it is 330 km. This difference in the sampled height can also allow for the larger phase angles detected here.

There are differences in the ranges and behaviour of the waves detected in the intensity and velocity curves between this work and Krijger et al. (2001). Nevertheless, both phase spectra, V-V and I-I (Figs. 4 and 5), show that high-frequency waves observed in this work do propagate upwards. At frequencies around 13 mHz the peak in the phase difference is noticeable (Figs. 4 and 5). To our knowledge, this is not observed in the previous work. This same peak is not so clear in the middle panel of Fig. 5. In both figures, (Figs. 4 and 5), it is obvious that above 13 mHz it is harder to establish the propagation. Similar behaviour is noted in the work by Krijger et al. (2001), but for different frequencies. Krijger et al. (2001) claims that this is due to steepening of high-frequency waves into weak shocks. Here such a statement cannot be confirmed. Our results give three possibilities: first, steepening into shocks; second, fast waves that have angles above 360 degrees; third, the behaviour is a consequence of the low signal resolution around those frequencies. Also, there are several possible theoretical interpretations for the behaviour of high-frequency waves observed here (Ulmschneider 2003, Kalkofen 1990, 2001, Wedemeyer-Böhm et al. 2007, Rosenthal et al. 2002, De Pontieu et al. 2004). Possibly the matter will be resolved in the future with instruments with higher temporal and spatial resolution.

Coherence distributions for each spectrum were calculated for the signal curves after the application of all conditions that were imposed to reduce spurious signals. Frequencies near the Nyquist frequency and frequencies below 1 mHz (DS1) and 2 mHz (DS2) were not cut out of the phase spectra and coherence distributions. Nevertheless, findings in those frequency ranges are not conclusive due to the unreliability of those ranges (see Section 2).

The distributions of the average velocities for the intensity and velocity signals, (Figs. 6 and 7) also confirm that there is a dominant trend for upward propagation. Stating finite numbers for phase velocities has to be done with caution. Apart from the influences of the solar conditions at the formation heights themselves (Asplund et al. 2000) there is also an influence caused by the post-focus instrumentation (Bendlin et al. 1992) and the effects of transmission of the telescope (Berkefeld et al. 2003). Therefore, all those factors have to be taken into account when discussing and analysing the results of the phase analysis. The phase angles show that there is propagation, but values of the propagation velocities are highly dependant on the assumed values for the height and therefore suffer from all of the problems connected with such assumptions. However, the values of the observed phase velocities are greater in the areas where magnetic structures appear for longer than half of the time series duration. The fact that propagation velocities are greater in the areas with significant magnetic concentrations is in agreement with the work by Rosenthal et al. (2002). These authors claim that, in the presence of the magnetic field concentration, the propagation velocities of high-frequency waves will be greater. Detection of the propagation in the low-frequency range, for the same data sample from DS2, is in agreement with the work by Jefferies et al. (2006) and De Pontieu et al. (2004). Both works claim that the presence of the magnetic field allows the low-frequency waves to propagate. However, since we did not have high resolution magnetograms for the data sets, the exact influence of the magnetic field cannot be established. Although there are indications that magnetic fields can be responsible for such behaviour, there is also a possibility that it is a consequence of the stochastic behaviour of the wave sources (Houdek et al. 1999). This question will be resolved with the high resolution magnetograms. Also, there is a significant difference in the diagrams of the intensity and velocity signals. This difference can be explained by the properties of the Radiative Transfer Equation (summary explanation with various references can be found in several chapters of the book by del Toro Iniesta 2003). In short, from a theoretical standpoint, velocity signals show waves clearer than intensity signals. However, this does not mean that results from the intensity are less reliable and that they can be ignored. The observed behaviour of both signals can help in improving the future atmospheric models that will deepen our understanding of the solar atmosphere.

Fig. 8 shows the phase spectrum calculated between velocity and intensity signals (V-I). All panels, except the bottom right one, show a clear tendency for waves to appear first in the velocity and then in the intensity signal. The top right panel (spectral line Fe I 543.29 nm, DS1), both middle panels (spectral lines Fe I 543.45 nm (left) and Fe I 543.29 nm (right), DS2), and the bottom left panel (spectral line Fe I 543.29 nm, DS2) show a tendency for positive phase angles. The trend for angles of $\approx 90^\circ$ for the low-frequency range 3 mHz – 6 mHz is found to be typical for evanescent waves in the work of Deubner et al. (1990). In Fig. 8, the middle left panel is the only one where this tendency can be seen for frequencies around 6 mHz. Therefore, we cannot certify this to be the typical behaviour for evanescent waves. Deubner and Fleck (1990) offer V-I phase diagrams for chromospheric lines which are significantly different from the V-I diagrams found here, indicating that the waves observed here do not exhibit the behaviour noted for the chromospheric waves. This difference might be caused by the heights sampled here. Although Deubner and Fleck (1989) sample photospheric and chro-

mospheric heights, the frequency ranges are difficult to compare with our results. As stated in Section 2, frequency ranges below 3 mHz might be influenced by the edge effects arising from the finite time span of our data. This gives us only frequencies 3 mHz - 5 mHz to compare. Unfortunately there is no visible agreement. Clear tendencies noticed by Deubner and Fleck (1989), Fleck and Deubner (1989) and Deubner et al. (1990) that indicate evanescent waves are not detectable in our data. It is possible that we do observe propagation of such waves, as predicted by De Pontieu et al. (2004) and commented on by Jefferies et al. (2006), as the possible cause of chromospheric heating. Comparing our results with works by Deubner and Fleck (1989, 1990), Fleck and Deubner (1989) and Deubner et al. (1990) can lead to the conclusion that we observe several different kinds of waves simultaneously, which is expected in light of recently developed multidimensional models and theoretical explanations of the solar atmosphere (Rosental et al. 2002, De Pontieu et al. 2004, Wedemeyer et al. 2004, Wedemeyer-Böhm et al. 2007).

In Figs. 4, 5 and 8 one can notice two clear streaks around frequencies below 3 mHz. As stated in Section 2, those ranges might be influenced by the edge effects arising from the finite time span of our data, therefore those ranges were excluded from discussion and analysis here.

The observed waves propagate upward in the frequency range 8 mHz – 13 mHz. We also noticed indications that in the lower-frequency range, below 8 mHz, there is an indication of the propagation in areas where the magnetic flux concentrations appear.

Acknowledgements – I am grateful to the Science and Technology Facilities Council for financial support. I especially, wish to thank Dr. N. Shchukina for calculating the formation heights for the lines used. Also, I wish to thank M. Mathioudakis and E. Wiehr for stimulating discussions. For help with the observations I wish to thank J. K. Hirzberger and K. G.Puschman. and F. Kneer for insisting on the importance of the research on these oscillations. Also I would like to thank A. M. Broomhall for advice on language.

REFERENCES

Andjic, A.: 2006, *Serb. Astron. J.*, **172**, 27.
Andic, A.: 2007a, *Solar Phys.*, **242**, 9.
Andic, A.: 2007b, *Solar Phys.*, **243**, 131.
Asplund, M., Nordlund, A., Tramperdach, R., Allende Prieto, C., Stein, R. F.: 2000, *Astron. Astrophys.*, **359**, 729.
Banerjee, D., O'Shea, E., Doyle, J. G., Goossens, M.: 2001, *Astron. Astrophys.*, **371**, 1137.
Bendlin, C., Volkmer, R., Kneer, F.: 1992, *Astron. Astrophys.*, **257**, 817.
Berger, T. E, Rouppe van der Voort, L. H. M., Löfdahl, M. G., Carlsson, M., Fossum, A., Hansteen, V. H., Marthinussen, E., Title, A., Scharmer, G.: 2004, *Astron. Astrophys.*, **428**, 613.
Berkefeld, Th., Soltau, D. von der L, O.: 2003, *Proceedings of the SPIE*, **4839**, 544.
Bloomfield, D. S., McAteer, R. T. J., Lites, B. W., Judge, P. G., Mathioudakis, M., Keenan, F. P.: 2004, *Astrophys. J.*, **617**, 623.
Bloomfield, D. S., McAteer, R. T. J., Mathioudakis, M., Keenan, F. P.: 2006, *Astrophys. J.*, **652**, 812.
Chatfield, C.: 2003, The Analysis of Time Series: An Introduction (Chapman and Hall Texts in Statistical Science Series), Chapman and Hall/CRC; 6th Ed edition, p. 352.
Davis, J. L.: 2000, Mathematics of Wave Propagation, Princeton University Press, p. 416.
del Toro Iniesta, J. C.: 2003, Introduction to Spectropolarimetry, Cambridge University Press, p. 227.
Deubner, F.-L., Fleck, B.: 1989, *Astron. Astrophys.*, **213**, 423.
Deubner, F.-L., Fleck, B.: 1990, *Astron. Astrophys.*, **228**, 506.
Deubner, F.-L., Fleck, B., Marmolino, C., Severino, G.: 1990, *Astron. Astrophys.*, **236**, 509.
De Pontieu, B., Erdélyi, R., James, S.P.: 2004, *Nature*, **430**, 536.
Emonet, T., Cattaneo, F.: 2001, *Astrophys. J.*, **560**, L197.
Fleck, B., Deubner, F.-L.: 1989, *Astron. Astrophys.*, **224**, 245.
Fossum, A., Carlsson, M.: 2006, *Astrophys. J.*, **646**, 579.
Ghosh, S. N.: 2002, Electromagnetic Theory and Wave Propagation, CRC Press Inc; 2nd Ed edition, p. 259.
Grenander, U.: 1959, Probability and statistics: The Harald Cramer volume (Unknown Binding), Almqvist and Wiksell; Wiley; Chapman and Hall, p. 434.
Houndek, G., Balmforth, N. J., Christensen-Dalsgaard, J., Gough, D. O.: 1999, *Astron. Astrophys.*, **351**, 582.
Jefferies, S. M., McIntosh, S. W., Amstrong, J. D., Bogdan, T. J., Cacciani, A., Fleck, B.: 2006, *Astrophys. J.*, **648**, L151.
Kalkofen, W.: 1990, In: Priest, E.R., Krishan, V. (eds.), Basic Plasma Processes on the Sun, *IAU Symp.*, **142**, 197.
Kalkofen, W.: 2001, *Astrophys. J.*, **557**, 376.
Krijger, J. M., Rutten, R. J., Lites, B. W, Straus, Th., Shine, R. A., Tarbell, T. D.: 2001, *Astron. Astrophys.*, **379**, 1052.
Lites, B. W., Chipman, E. G.: 1979, *Astrophys. J.*, **231**, 570.
Mathioudakis, M., Seiradakis, J. H., Williams, D. R., Avgoloupis, S., Bloomfield, D. S., McAteer, R. T. J.: 2003, *Astron. Astrophys.*, **403**, 1101.
McAteer, R. T. J., Gallagher, P. T., Bloomfield, D. S., Williams, D. R., Mathioudakis, M., Keenan, F. P.: 2004, *Astrophys. J.*, **602**, 436.
Parker, E. N.: 1978, *Astrophys. J.*, **221**, 368.
Phillips, K. J. H.: 1992, Guide to the Sun, Cambridge University Press, p. 386.
Rosenthal, C. S., Bogdan, T. J., Carlsson, M., Dorch, S. B. F., Hansteen, V., McIntosh, S. W., McMurry, A., Nordlund, A., Stein, R. F.: 2002, *Astrophys. J.*, **564**, 508.

Shchukina, N. G., Trujillo Bueno, J.: 2001, *Astrophys. J.*, **550**, 970.
Stein, R. F., Leibacher, J.: 1974, *Astron. Astrophys.*, **12**, 407.
Thio, T.: 2006, *American Scientist*, **94**, 40.
Title, A. M., Schrijver, C. J.: 1998, *in ASP Conf. Ser.*, **154**, The Tenth Cambridge Workshop on Cool Stars, Stellar Systems and the Sun, ed. R. A. Donahue, J. A. Bookbinder (San Franciso: APS), 345.
Torrence, C., Compo, G. P.: 1998, *Bull. Amer. Meteor. Soc.*, **79**, 61.
Ulmschneider, P.: 1971a, *Astron. Astrophys.*, **12**, 297.
Ulmschneider, P.: 1971b, *Astron. Astrophys.*, **14**, 275.
Ulmschneider, P.: 2003, Review: the physics of chromosphere and corona. In: Lectures in solar Physic, H. M. Antia, Springer and Verlag.
van Ballegooijen, A. A., Hasan, S. S.: 2003, Preparing for ATST ASP Conference Series, Vol. 286.
Wang, Z., Urlich, R. K., Coroniti, F.V.: 1995, *Astrophys. J.*, **444**, 879.
Wedemeyer, S., Freytag, B., Steffen, M., Ludwig, H.-G., Holweger, H.: 2004, *Astron. Astrophys.*, **414**, 1121.
Wedemeyer-Böhm, S., Steiner, O., Bruls, J., Rammacher, W.: 2007, arXiv:astro-ph **0612627v1**

ПРОСТИРАЊЕ ВИСОКОФРЕКВЕНЦИОНИХ ТАЛАСА У ТИХОЈ СУНЧЕВОЈ АТМОСФЕРИ

A. Andić[1,2]

[1] *HiROS, School of Physics and Astronomy, College of Engineering and Physical Sciences, The University of Birmingham, Edgbaston, Birmingham, B15 2TT, UK*

[2] *Astrophysics Research Centre, School of Mathematics and Physics, Queen's University, Belfast, BT7 1NN, UK*

E–mail: *andic@bison.ph.bham.ac.uk*

УДК 523.94–78
Оригинални научни рад

Високофреквенциони таласи (5 - 20 mHz) су предложени као извор грејања тихе сунчеве атмосфере. Динамика тих, раније детектованих таласа је представљена овде. Секвенце слика су добијене коришћењем Фабри-Перо спектрометра лоцираног у њемачком Вакуумском Торањ-Телескопу (VTT) на Обсерваторији дел Теиде, Изана, Тенерифе. Подаци су потом редуковани спекле методом и анализирани веувлетима. Да се утврди да ли се посматрани таласи простиру, извршена је анализа фазне разлике базирана на веувлетима. Забележили смо простирање таласа у фреквенционом опсегу од: 10 mHz то 13 mHz. Такође, забележено је простирање таласа у фреквенционим опсезима где се ти таласи иначе не простиру, на локацијама где су биле присутне магнетне структуре.